**PAPER** • **OPEN ACCESS**

# Warming structure of the Kuroshio in the East China Sea since 1970

Environmental Research Communications

PAPER

# Warming structure of the Kuroshio in the East China Sea since 1970

**Xiaoqian Li**[1,2], **Yuanlong Li**[2,3,4], **Kai Ge**[2,3], **Xiaohui Tang**[2,4], **Shouhua Liu**[5] **and Shanliang Zhu**[1]

[1] School of Mathematics and Physics, Qingdao University of Science and Technology, Qingdao 266061, People's Republic of China
[2] Key Laboratory of Ocean Observation and Forecasting and Key Laboratory of Ocean Circulation and Waves, Institute of Oceanology, Chinese Academy of Sciences, Qingdao 266071, People's Republic of China
[3] University of Chinese Academy of Sciences, Beijing, People's Republic of China
[4] Laboratory for Ocean Dynamics and Climate, Qingdao Marine Science and Technology Center, Qingdao, People's Republic of China
[5] National Marine Data and Information Service, Ministry of Natural Resources, Tianjin 300171, People's Republic of China

**E-mail:** tangxiaohui@qdio.ac.cn

**Keywords:** Kuroshio Current, East China Sea, surface warming, subsurface cooling

Supplementary material for this article is available online

**OPEN ACCESS**

**RECEIVED**
11 December 2024

**REVISED**
31 January 2025

**ACCEPTED FOR PUBLICATION**
28 February 2025

**PUBLISHED**
12 March 2025



## Abstract

The Kuroshio Current (KC) has witnessed rapid surface warming during the past half-century, impacting the marine ecosystems in surrounding regions. However, the vertical structure of the warming KC remains unclear. This study utilizes historical hydrographic observational data and ocean model experiments to investigate temperature changes of the KC in the East China Sea since 1970. The KC at the Pollution Nagasaki (PN) section has shown rapid warming in the upper 350 m and insignificant warming or cooling trends in the subsurface layer of 350–800 m. Our diagnosis suggests that the rapid upper-layer warming results from the downward displacement of isopycnal surfaces, whereas the subsurface cooling arises from lateral advection along isopycnal surfaces. In addition to surface heating, surface wind changes over the subtropical North Pacific-induced by the phase shift of the Pacific Decadal Oscillation (PDO)-also enhance the upper-layer warming of the KC by driving downwelling Rossby waves. The subsurface cooling reflects property changes of the North Pacific Intermediate Water (NPIW) which can be traced to buoyancy fluxes in the subpolar northwestern Pacific. By linking the regional changes observed in the ECS to basin-scale processes over the North Pacific, this work contributes to the understanding of the response of the KC to climate change.

## 1. Introduction

The East China Sea (ECS) possesses one of the largest continental shelves of the world's oceans, harboring economically important ecosystems. The ECS has shown rapid surface warming trends since the mid-20th century (Xie *et al* 2002, Tang *et al* 2009, Xu *et al* 2011, Miyama *et al* 2012). This persistent warming has led to more frequent and intense marine heatwaves, exacerbating the stress of climate change on marine ecosystems and coastal biological systems (Cai *et al* 2016, Wang *et al* 2023). In addition to changes in the East Asian monsoon (D'Arrigo *et al* 2005, Xu *et al* 2006, Yeh and Kim 2010, Cai *et al* 2017), the increase in heat transport from the Kuroshio Current (KC) is also a major driver of the rapid ECS warming (Zhang *et al* 2010, Rudnick *et al* 2011, Wu *et al* 2012). Originating from the bifurcation of the North Equatorial Current (Qiu and Lukas 1996), the KC flows northeastward along the continental slope situated in the offshore part of the ECS (Nitani 1972). The KC communicates with the Yellow Sea and ECS shelves through intrusive flows, playing a crucial role in the heat and material budgets of these regions (Hsueh 2000, Yuan *et al* 2008, Oey *et al* 2013, Chen *et al* 2021). Temperature change in the KC modulates typhoon genesis (Wu *et al* 2008), fishery production (Tsukamoto 2006), and hydrographic structure (Hsin *et al* 2013, Wu 2013) of the Northwest Pacific Ocean and marginal seas and potentially affects the global climate (Kwon *et al* 2010).

Notable and complex changes in the KC have been witnessed in the ECS during the past decades (Andres *et al* 2009, Soeyanto *et al* 2014, Wu *et al* 2019, Qiao *et al* 2022). There has been an overall increasing trend of the KC volume transport at the Pollution Nagasaki (PN) section (from 30°N, 124.5°E to 27.5°N, 128.25°E) since 1955

(Wei *et al* 2013, Zhu *et al* 2015), which is superimposed by prominent decadal variability. For example, the KC weakened during 1993–2013 and meanwhile caused increased warm-water intrusion into the ECS shelf (Hsin *et al* 2013, Wu 2013). Changes in the KC strength are primarily controlled by the basin-scale surface wind field over the North Pacific (Wang *et al* 2016). In the late-1990s, the Pacific Decadal Oscillation (PDO) shifted from the positive to the negative phase, leading to enhanced Walker Circulation in the tropical Pacific (Kosaka and Xie 2013, Trenberth *et al* 2014, England *et al* 2014) and weakened westerlies (Mantua and Hare 2002). In addition, typhoons and mesoscale eddies generated in the Northwest Pacific Ocean also potentially modulate the KC strength in the ECS (Yan *et al* 2019, Zhang *et al* 2021). The KC in the ECS has shown a striking surface warming trend, which intensified the warming of the ECS shelf through heat advection (Oey *et al* 2013, Sasaki and Umeda 2021, Yu *et al* 2012). Wu *et al* (2012) revealed that the accelerated surface warming is associated with the poleward migration of the KC in conjunction with surface wind changes.

Compared to surface temperature, changes in subsurface temperatures of the Kuroshio are much less visited. The Kuroshio in the ECS carries different water masses in different layers, including the warm, low-salinity surface water above 100 m, the high-salinity North Pacific Tropical Water (NPTW) between 100–300 m, and the cold, low-salinity North Pacific Intermediate Water (NPIW) at 400–800 m (Qu *et al* 1997, Li and Wang 2012a). Controlled by different processes, these waters may exhibit differential property changes, exerting complex impacts on the ECS. Based on empirical orthogonal function (EOF) decomposition analysis, Pei *et al* (2017) demonstrated that warming trend at the PN section decreases steadily with depth and even shifts to a cooling trend in the intermediate layer. Stronger warming of surface water than subsurface waters may lead to enhanced ocean stratification. This inhibits vertical exchanges of carbon, dissolved oxygen, and nutrients (Li *et al* 2020) and thereby increases the severity of hypoxia and acidification in the ECS coastal waters (Li *et al* 2014, Chi *et al* 2017). A decline in phytoplankton biomass has been observed in the ECS since 2000, linked to enhanced ocean stratification due to surface warming (Wang *et al* 2023). Therefore, to better understand the long-term change of the KC and its impact on the ECS, it is necessary to explore the vertical structure of the warming KC.

In this study, we investigate the warming structure of the ECS Kuroshio and the underlying processes. Analysis of repeated *in situ* measurement data at the PN and gridded observational data reveals strong upper-layer warming and weaker lower-layer cooling in the ECS Kuroshio. Through thermodynamic diagnosis and ocean model sensitivity experiments, we further elucidate different mechanisms governing the two layers. Our results successfully attribute regional changes in the ECS to basin-scale dynamic and thermodynamic processes over the North Pacific, providing implications for the prediction of environmental changes in marginal seas in a warming climate.

## 2. Data and methods

### 2.1. Observational data

To characterize temperature changes in the ECS Kuroshio, we utilize repeated *in situ* measurements of 1970–2020 along the PN section (Oka and Kawabe 1998) provided by the Japan Meteorological Agency (JMA). The PN section is a standard section that crosses the main axis of the Kuroshio in the middle of the ECS, extending from the northwest corner near the Yangtze River estuary to the southeastern Ryukyu Islands in a northwest-southeast direction. We collected temperature profiles at the 16 hydrographic stations in the southeastern part of the PN section (figure 1(a)), from 29°N, 126°E in the west to 27.5°N, 128.25°E in the east, that have been regularly surveyed till present (the same stations as in Wei *et al* 2013). Temperature was measured with Nansen bottle at standard depths before 1986, and with conductivity-temperature-depth (CTD) since 1987. The data analyzed here, 2972 profiles in all, are mostly collected during 1972–2008, with relatively uniform distribution across different seasons (e.g., December, January, and February are adopted as boreal winter). After a quality control removing profiles with evident errors, we constructed seasonal temperature series by averaging all available profiles at each station for each season, each year. Then, seasonal fields were averaged into annual-mean fields for our analysis. The temperature change shown in figure 1(c) is calculated as the difference between the average annual-mean field of 1990–2020 and that of 1970–1990. The statistical significance of the change is determined through a two-sided student's t-test.

To explore large-scale oceanic changes linked to changes observed in the Kuroshio, we analyze the Institute of Atmospheric Physics (IAP) oceanic analysis data of 1970–2020 (Cheng *et al* 2017, 2024). This dataset provides 0.5° × 0.5°, standard-level monthly temperature and salinity fields of the 0–2000 m global ocean. We also analyze the 0.25° × 0.25° Ssalto/Duacs satellite sea surface height (SSH) data of 1993–2020 distributed by the Copernicus Marine and Environment Monitoring Service (CMEMS) and 10-m winds from the fifth generation European Centre for Medium-Range Weather Forecasts reanalysis (ERA5) of 1970–2020 (Hersbach *et al* 2023). The 5′ (1/12°) terrain data from Earth's Topography and Bathymetry (ETOPO5) was also used (National Geophysical Data Center, NESDIS, NOAA, U.S. Department of Commerce 1986). The Pacific Decadal

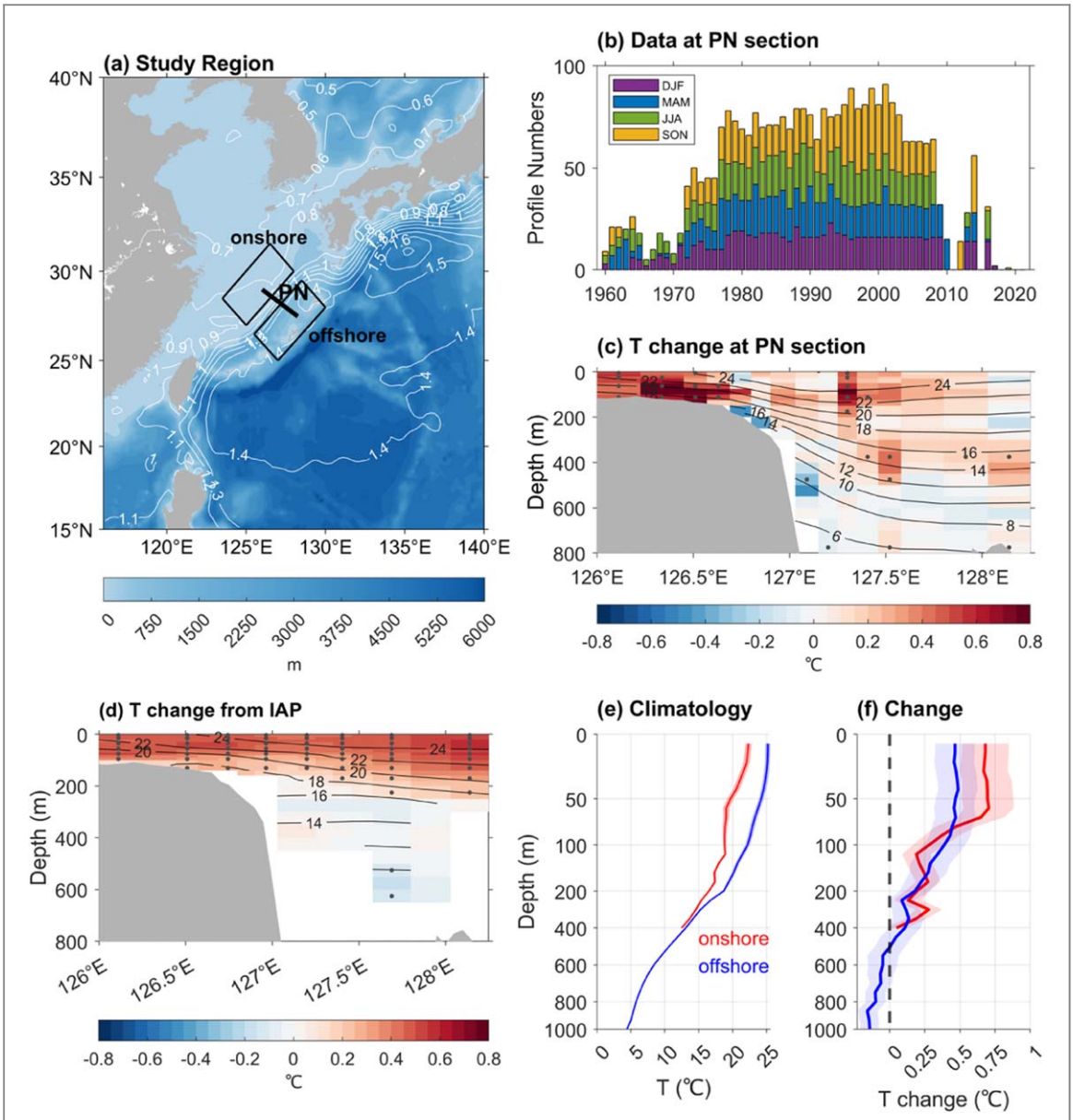


**Figure 1.** (a) Topography of the northwest pacific ocean (NWPO) and adjacent seas based on the ETOPO5 data. The white contours denote the annual-mean climatological sea surface height (m) of 1993–2020, derived from CMEMS data. The thick black line remarks the PN section for the Kuroshio in the ECS, and the black rectangles denote the onshore and offshore boxes, respectively. (b) Annual data profile number of repeated hydrological observation at the PN section from JMA. Data collected in different seasons (e.g., DJF: December, January, and February) are plotted in different colors. (c), (d) Temperature change (color shading) and climatological temperature (black contours) of 1970–2020 at the PN section, based on JMA data in (c) and the Chinese Academy of Sciences/ Institute of Atmospheric Physics (IAP) ocean analysis (d). The change is calculated as the difference between the 1990–2020 and the 1970–1990 periods. The stippling in (c) and (d) indicates significant changes at the 90% confidence level, based on a student's t-test. Profiles of (e) annual-mean climatological temperature and (f) temperature change at depth averaged over the onshore (red) and offshore (blue) boxes, derived from the IAP data. The shading indicates the one standard deviation range of temperatures at different grid points for (e) and the 90% confidence interval of the change in (f).

Oscillation (PDO) Index is based on NOAA's extended reconstruction of SSTs (Zhang *et al* 1997, Huang *et al* 2017).

### 2.2. Diagnosis of causing factors

Causing factors for ocean subsurface temperature changes seen at depth levels can be diagnosed by calculating 'heaving' and 'spicing' (Bindoff and McDougall 1994, Huang 2020). In the subsurface ocean, waters are assumed to move along isopycnal surfaces. Therefore, analyzing changes of isopycnal surfaces provides insights into key processes causing subsurface ocean temperature changes. Specifically, the 'heaving' is associated with vertical displacements of isopycnal surfaces arising from adiabatic convergent/divergent motions induced by wind forcing and ocean internal instabilities and diabatic heating of seawater (Häkkinen *et al* 2016, Lu *et al* 2024). The 'spicing' manifests compensated temperature and salinity changes along isopycnal surfaces, representing the

modification of water-mass properties (Bindoff and McDougall 1994). The temperature change of spicing is induced by lateral advection along isopycnal surfaces. Practically, the ocean subsurface temperature (or salinity) change at depth levels ΔT|z can be explained by either spicing or heaving (Durack and Wijffels 2010, Häkkinen *et al* 2016),

$$\Delta T|_z = \Delta T|_\sigma + \frac{\partial \bar{T}}{\partial \bar{\sigma}}|_z, \tag{1}$$

where $\Delta T|_\sigma$ represents the temperature change on isopycnal (with a potential density of $\sigma$) surfaces interpolated onto depth levels, which quantifies the spicing. The second term on the right represents the temperature changes caused by vertical displacement of isopycnal surfaces, as a representation of heaving, where $\frac{\partial \bar{T}}{\partial \bar{\sigma}}$ is the diapycnal temperature gradient in climatology and $\Delta\sigma|_z$ is the potential density change seen at depth levels.

### 2.3. LICOM3 simulations

In this study, we use the Laboratory of Atmospheric Sciences and Geophysical Fluid Dynamics (LASG)/IAP Climate Ocean Model (LICOM) Version-3 (Lin *et al* 2020) to simulate and understand the ocean temperature change (Gao *et al* 2023, Lu *et al* 2024). The LICOM simulation adopts a tripolar grid of global domain with horizontal resolutions of $1^\circ \times 1^\circ$. 3-hourly surface atmospheric fields of ERA5 are adopted as the surface forcing of LICOM. A spin-up run of 500 years was first conducted, forced by repeated ERA5 3-hourly atmospheric fields of 1941–1950. Restarted from the already spun-up solution, the model was integrated from 1941 to 2020 under realistic hourly ERA5 fields to form the control run (CTR). CTR contains full processes controlling ocean temperature change and is compared against observational data to validate the model performance. The LICOM data consists of 30 vertical layers, with depths ranging from 5 to 5243 m.

In parallel with CTR, three 'single-forcing' experiments were performed to explore the causes of ocean temperature changes. The wind run (WND) keeps only the changes in surface winds, with other forcing fields (radiations, precipitation, air temperature, and air humidity) fixed to the 1941–1950 cycles as in the spin-up run. This experiment contains forcing effects of both dynamical processes controlled by wind stress change and latent and sensible heat fluxes controlled by wind speed. Similarly, the precipitation run (PRCP) retains changes in precipitation rate and fixes all other forcing fields to 1941–1950 cycles. As such, ocean temperature changes in PRCP arise from precipitation-driven salinity changes that alter ocean stratification (Liu *et al* 2021) and properties of subducted water masses (Bindoff and McDougall 1994). In the heat flux run (HTFL), both wind and precipitation are fixed to 1941–1950 cycles, while other forcing fields are the same as in CTR. As such, HTFL simulates ocean temperature changes driven by time-varying shortwave and longwave radiations, air temperature affecting sensible heat flux, and air humidity affecting latent heat flux.

## 3. Results

### 3.1. Warming structure of the ECS Kuroshio

We first look at the observed warming structure of the ECS Kuroshio since 1970, derived from historical observational data of JMA at the PN section (figure 1(c)). We find that significant warming signatures are mainly trapped above 400 m, showing rapid surface warming trends in the ECS shelf west of 127°E. The maximum warming since 1970 exceeds 0.8 °C. Below 400 m, there are weaker warming and even cooling trends east of 127°E. There, the warming rate ranges from ~ −0.2 to ~ 0.6 °C and is insignificant in most areas of 400–800 m. At the continental slope between 126.5°E and 127°E, there is a sharp inclination of climatological isotherms, reflecting the baroclinic structure of the geostrophic KC. The strongest cooling signal appears near the continental slope and is significant at the 90% confidence level at ~ 500 m. These structures suggest that the cooling signal may be carried by the KC to the bottom of the ECS shelf through cross-shelf intrusion (Zhou *et al* 2015, Zhang *et al* 2017), potentially impacting the ECS.

To gain insights into large-scale processes, we adopt IAP data for further analysis. Here, we first interpolated IAP data onto the PN section (figure 1(d)). Like JMA data, the IAP data shows surface-intensified upper-layer warming and an overall cooling trend below 400 m. Compared to JMA data, the upper-layer warming in IAP data is much more uniform, lacking surface intensification. Also, the IAP data fails to capture the strong cooling near the bottom of the continental slope. This is mainly due to the construction approach of the 0.5° IAP dataset, the interpolation and gap-filling lead to smooth fields in IAP data and a failure to resolve regional characteristics over complex topography. Although with shortcomings in resolving detailed features, IAP data provides reliable insights into large-scale characteristics of the warming structure of the ECS Kuroshio.

We further analyze the average temperatures of the onshore and offshore boxes of the PN section (figure 1(a)). In climatology, the offshore side of the KC is warmer than the onshore side by 3 °C–4 °C (figure 1(e)) in the upper 200 m, a characteristic reflecting the thermal wind relationship of the geostrophic KC.

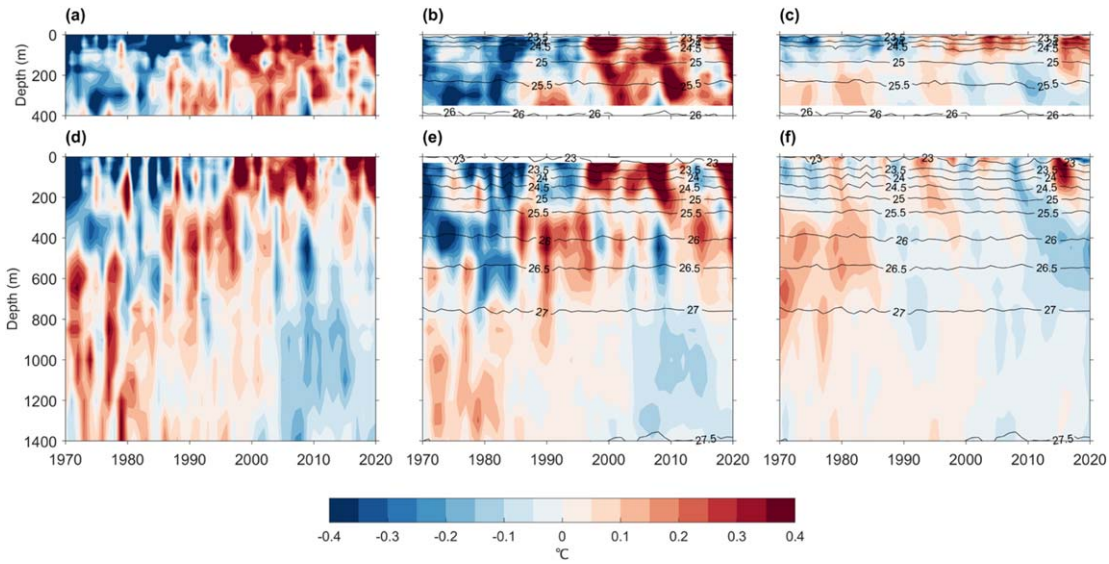


**Figure 2.** Temperature anomalies of heaving and spicing. (a), (d), Total temperature anomalies averaged over the onshore (a) and offshore (d) boxes. (b)–(f), Temperature anomalies averaged over the onshore (b), (c) and offshore (e), (f) boxes in the heaving (b), (e) and spicing (c), (f), where the black contours denote the climatological isopycnal surfaces of 23.0–27.0 kg m$^{-3}$ with a 0.5 kg m$^{-3}$ interval. Here, anomalies are calculated relative to the 1970–2020 baseline.

The temperature changes of the surface layer within 70 m from 1970–1990 to 1990–2020 are 0.65 ± 0.16 °C and 0.47 ± 0.14 °C in the onshore and offshore boxes, respectively. The warming rate decreases with depth, reducing to 0.19 ± 0.08 °C and 0.18 ± 0.11 °C at 200 m in the inshore and offshore boxes, respectively. Below 400 m, there is a cooling trend emerging in the offshore box, reaching up to −0.1 ± 0.08 °C at 800 m (figure 1(f)).

Next, we examine the temporal evolution of temperature anomaly profiles of the onshore and offshore boxes (figures 2(a) and (d)). In both boxes, the upper layer of 0–350 m shows an abrupt shift from cold to warm anomalies in the late 1990s. Superimposed upon an overall warming trend, there are strong interannual and decadal fluctuations. The offshore box shows a cooling trend in the subsurface layer, which is particularly prominent below 500 m. To gain insights into the causes of the KC's warming structure, we perform the diagnosis heaving and spicing (section 2.2) (figures 2(b)–(f)). The diagnosis using IAP data suggests that although both heaving and spicing exhibit warming trends in the upper layer, the contribution of heaving is greater than that of spicing. Furthermore, the temperature shift in the late 1990s mainly occurs in heaving. In contrast, the warming trend in spicing is weaker, subjected to strong interannual variability, and mainly confined to the near-surface layer of $< 25.0$ kg m$^{-3}$ in potential density. The subsurface cooling trend primarily occurs in spicing, showing up below 300 m, and is particularly prominent in the 25.5–27.0 kg m$^{-3}$ layer.

The warming structures we found above can be briefly depicted by the time series of temperature anomaly of the onshore and offshore boxes at different layers (figure 3). The apparent ascending tendency of the temperature anomalies at 0–300 m in both boxes (figures 3(a) and (b)) and their weak correlations to the PDO (−0.1242 and −0.0605) suggest that the upper-layer warming trends of the ECS Kuroshio are likely driven by anthropogenic climate change rather than natural climate fluctuations. Nevertheless, it does not necessarily mean that the abrupt shift from cold to warm anomalies around 1997 (seen in figures 3(a)–(d)) are not influenced by natural variabilities. On the other hand, the temperature variability at 300–800 m of the offshore box shows considerable interdecadal fluctuations superimposed on a cooling trend (figure 3(c)). Its moderate correlation with the PDO (0.2612) is mainly reflected in the interdecadal variability of subsurface heaving (figure 2(e)), yet cannot explain the cooling trend in spicing (figure 2(f)). Therefore, the underlying mechanism causing the upper-layer temperature shift around 1997 and the subsurface cooling trend need to be further investigated in perspective of large-scale oceanic processes.

### 3.2. Processes associated with heaving

Analysis of observational data presented above reveals an upper-layer warming and a subsurface cooling of the ECS Kuroshio, residing mainly in heaving and spicing, respectively. In this subsection, we explore processes underlying the rapid warming of the upper 350 m, such as diabatic heating through surface heat uptake and heat redistribution induced by changes in surface winds (Garuba and Klinger 2016, Duan *et al* 2023, Ren *et al* 2024). The wind stress curl (WSC), calculated as WSC $= \partial\tau_y/\partial x$ - $\partial\tau_x/\partial y$, where $\tau_x$ and $\tau_y$ are zonal and meridional wind stress, respectively, represents the forcing effect by surface winds on the upper ocean (Qiu and Lukas 1996).

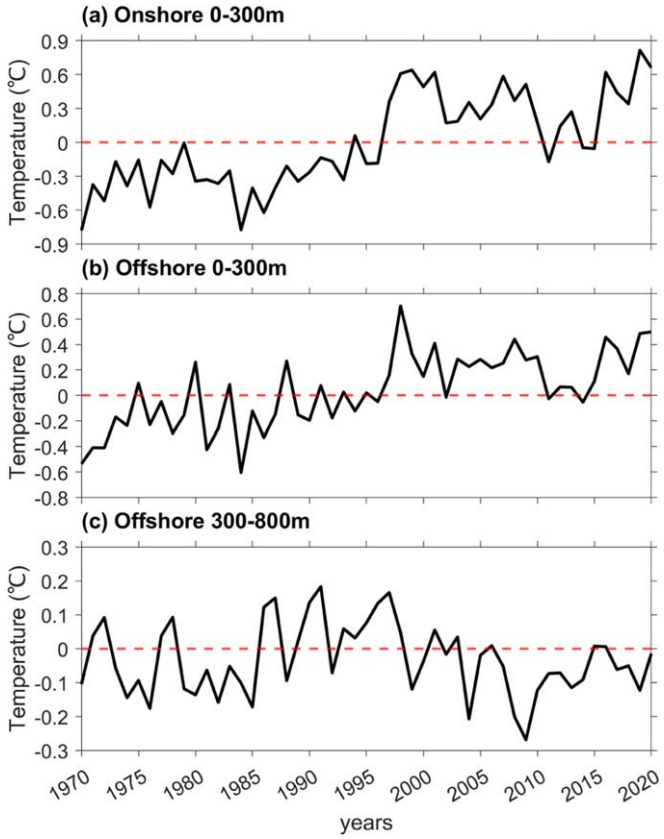


**Figure 3.** Time series of temperature anomalies of 1970–2020 averaged in: (a) the onshore box (0–300 m), (b) the offshore box (0–300 m), and (c) the offshore box (300–800 m).

In climatology, the subtropical North Pacific is controlled by basin-wide anticyclonic winds, characterized by negative WSCs (figure S1a). During 1970–2020, there are trends of anticyclonic winds and negative WSCs in the northeast subtropical Pacific of 170°–120°W (figure S1b). Negative WSCs can cause upper-layer convergence of warm water in the Northern Hemisphere, which is conducive to the warming of the upper ocean. However, in the central subtropical North Pacific of 150°E–170°W, there are trends of positive WSCs that can cause upper ocean cooling.

To better understand the response of the upper ocean to surface wind changes, we produce time-longitudinal plots of the 0–350 m average temperature anomalies and WSC anomalies in the 25°–30°N band where the ECS Kuroshio is located (figure 4). The warming near the western boundary, especially the abrupt warming in the mid-1990s, can be tracked to regions east of 170°W (figure 4(a)). The negative WSC trends between 170°–120°W seen in figure S1b likely stem from the positive WSC anomalies of 1977–1997 and the negative WSC anomalies of 1998–2014 (figure 4(b)). These changes arise from the shift of PDO from the positive to negative phase during 1997–1998 (figure 4(c)). After 1997, negative WSC anomalies drove westward-propagating downwelling Rossby waves, resulting in upper-layer warming in the central and western Pacific (figure 4(a)). In fact, the warming signatures diminish as approaching the western boundary, owing to the damping effect of local positive WSC anomalies. Despite this, downwelling Rossby waves ultimately enhanced the upper-layer warming of the ECS Kuroshio. In contrast, the eastern basin between 170°–120°W experienced cooling, caused by upwelling Rossby waves originating from positive WSC anomalies near the eastern boundary.

This analysis presented above points to the essence of wind-driven oceanic processes in the warming. To confirm this, we conducted experiments using LICOM (section 2.3). The simulated upper-layer temperature changes in CTR are consistent with IAP data in the time-longitude plot (figure S2a). Changes in sea surface height (SSH) (figure S2b) resemble those in ocean temperature in spatial and temporal characteristics, showing westward propagating anomalies that conform to behaviors of baroclinic long Rossby waves. Some anomalies do not show evident westward propagating characteristics or are not continuous, suggesting that local wind forcing in the western Pacific may also play a role in causing the observed changes. Further, SSH anomalies in the WND experiment, driven only by surface wind changes (figure S2c), are highly consistent with those in CTR.

LICOM CTR agrees with observation (IAP) in representing temperature changes in the upper 350 m induced by heaving (figure 5(a) and figure S3). CTR broadly captures the observed warming features north of

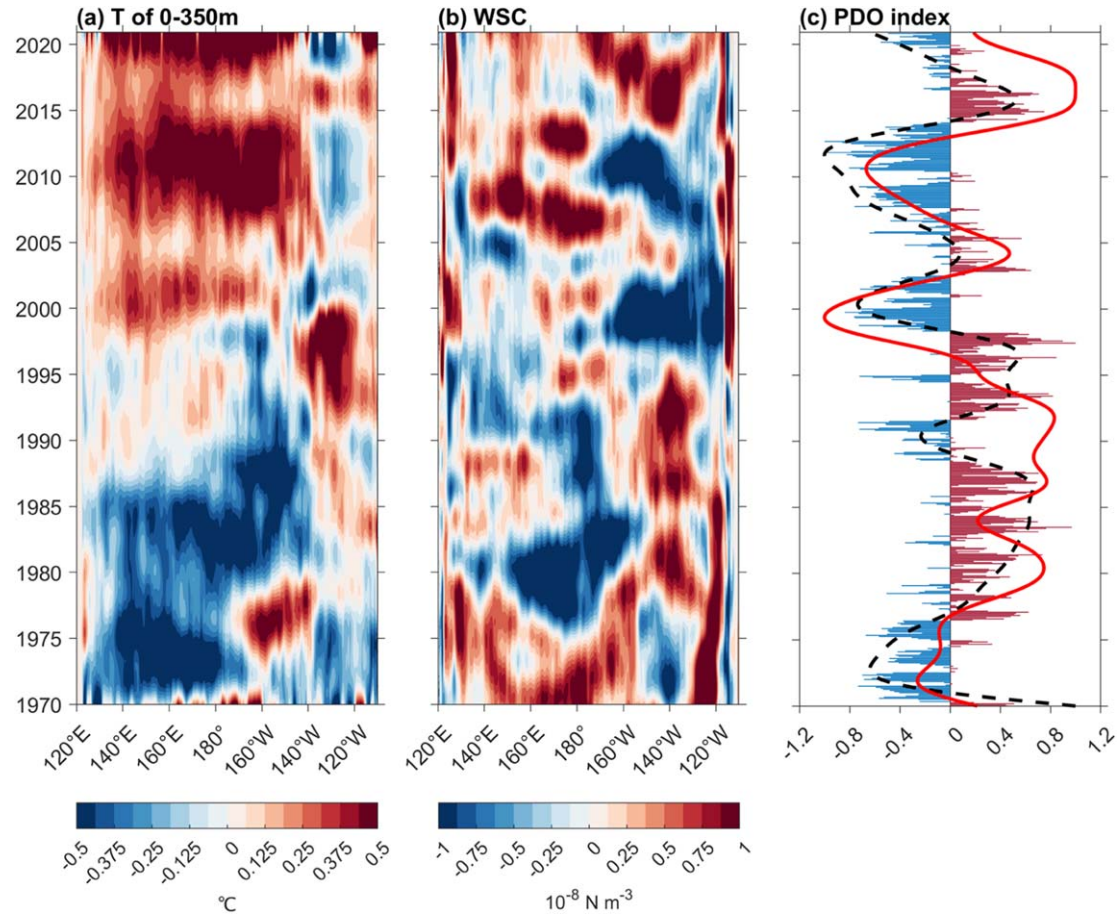


**Figure 4.** Time-longitude plots of (a) the average temperature anomaly (°C) of the upper 350 m and (b) wind stress curl (WSC) anomaly ($10^{-8}$ N $m^{-3}$) along the 25°N–30°N band. Both (a) and (b) are low-passed filtered with a 6-year Hanning window. (c) The monthly (bars) and 6-year low-passed (black dashed line) PDO index, are derived from ERSST. The red line represents the average WSC, in the region of 155°W–135°W, 25°N–30°N, with a 6-year low-pass filter applied. Both the PDO index and WSC are normalized.

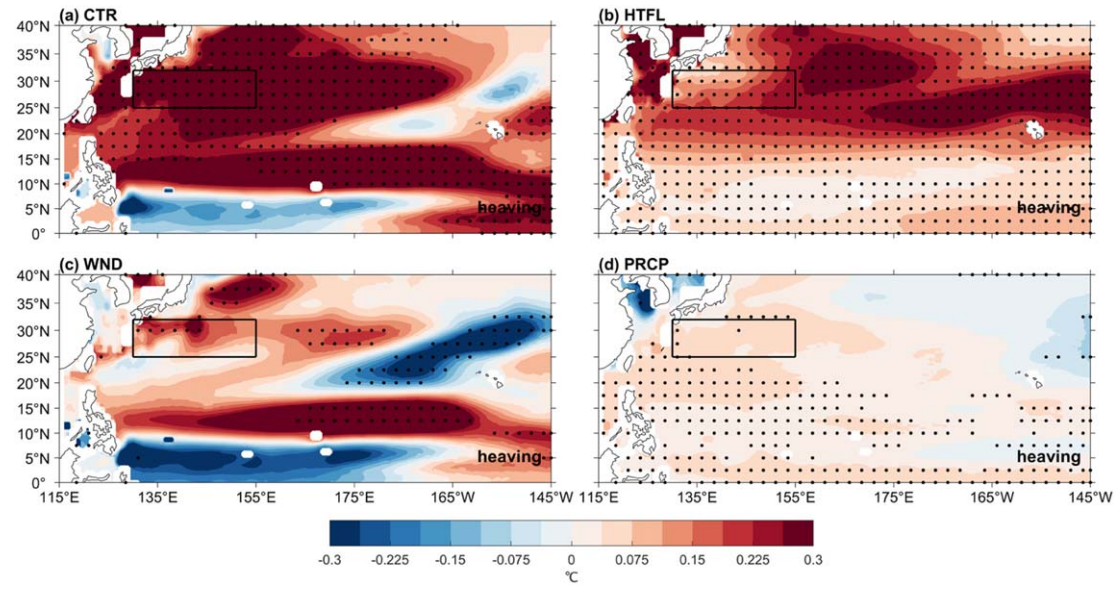


**Figure 5.** The 0–350 m temperature change of 1970–2020 in heaving, derived from CTR (a), HTFL (b), WMD (c) and PRCP (d) simulations of LICOM. Stippling indicates significant changes at the 90% confidence level. The area-average change is calculated for the subtropical NWPO region of 130°E–155°E, 25°N–32°N (black rectangle).

25°N and west of 180° in the North Pacific. Most of the warming signatures across the subtropical North Pacific are significant at the 90% confidence level. However, CTR fails to reproduce the cooling signals in the Kuroshio Extension region east of Japan, likely owing to its coarse resolution. Similarly, it is difficult to accurately capture the complex topography and flow structure of the ECS Kuroshio. Temperature changes in the ECS Kuroshio are consistent with, and physically linked to, large-scale changes of the subtropical northwestern Pacific Ocean (NWPO, 130°E-155°E, 25°N -32°N), since changes in this region converge into the Kuroshio through the gyre. Therefore, the following analysis using LICOM experiments will focus on the NWPO region, rather than the ECS Kuroshio, to achieve insights into the large-scale oceanic processes that potentially contribute to the warming structure of the ECS Kuroshio.

To separately evaluate the contributions of winds, heat flux, and freshwater flux to upper-layer warming, we analyzed the upper 350 m temperature changes of heaving from the LICOM single-forcing experiments (figure 5). The results suggest that the prevailing upper-layer warming in the NWPO (figure 5(a)) is jointly driven by surface heating and wind forcing (figures 5(b) and (c)), and in comparison, changes in precipitation rate have a much smaller contribution (figure 5(d)). The HTFL experiment suggests that surface heat flux causes widespread warming across the North Pacific, with significantly stronger warming in the subtropical region (15°–35°N) than the tropical region south of 15°N (figure 5(b)). This warming pattern shaped by surface heat uptake is consistent with the heat storage under anthropogenic greenhouse warming projected by climate models (Cheng *et al* 2022, Duan *et al* 2023). Yet, this pattern is insufficient to explain the strong warming in observation or CTR. The WND experiment shows that changes in surface winds led to a redistribution of warm water across the North Pacific. One of the regions of warm water convergence is located between 25°N and 32°N in the western Pacific, aligning with the latitude band where a negative wind stress curl (WSC) trend appears (figures 4 and S1). A similar pattern is observed between 10°N and 15°N, where a negative WSC trend is also present in the east. Changes in precipitation affect ocean temperatures mainly by altering the ocean stratification (figure not shown) and thereby modulating heat uptake (Liu *et al* 2021). In the NPWO region, contributions of WND, HTFL, and PRCP to the total warming in CTR are 34%, 49%, and 11%, respectively. The contribution percentages are calculated by the ratio of the temperature changes in the NPWO region for the HTFL, PRCP, and WND experiments, respectively, to that of the CTR experiment. These results based on LICOM experiments confirm the essential role of surface wind changes (partly arising from PDO phase shifts), in addition to surface heating, in causing the upper-layer warming of the NWPO through driving convergence of warm water.

### 3.3. Processes associated with spicing

In this subsection, we explore processes underlying the subsurface cooling trend that occurs as the spicing. In the NPTW layer of 23.5–24.5 kg $m^{-3}$ (Li *et al* 2012b), both IAP and CTR show weaker warming trends in the NWPO (figures 6(a) and (b)). These trends reflect the warming and salinity increase (figures S4a and S4b) of the NPTW in this region. CTR captures the spatial pattern of density-compensated temperature and salinity changes of the NPTW, which manifests as spicing in the ECS Kuroshio region. Along isopycnal surfaces of 26.0–26.7 kg $m^{-3}$, there are significant cooling trends over most parts of the subtropical North Pacific basin, primarily occurring between 400 and 600 m (figure 6(c)). These trends mainly reflect the cooling and freshening (figure S4c) trends of the NPIW (Wong *et al* 1999, Durack and Wijffels 2010) that is originated from the subpolar North Pacific. Temperature and salinity changes in the 26.0–26.7 kg $m^{-3}$ layer generally align with observations (figures 6(d) and S4d), although slightly stronger warming is simulated in the eastern Pacific (figure 6(d)). The cooling in the 26.0–26.7 kg $m^{-3}$ layer enters the ECS Kuroshio via the mean circulation as passive tracers, as seen in observation (figures 1 and 2). The consistency between IAP and CTR lends us the confidence to use LICOM single-forcing experiments to seek candidate drivers for subsurface cooling.

We further examine changes in the PRCP, WND, and HTFL experiments of LICOM. In the NPTW layer of 23.5–24.5 kg $m^{-3}$, warming near the ECS Kuroshio is only seen in HTFL (figures 7(a)–(e). This highlights the dominance of surface heating in causing the warming of the NPTW in the western Pacific. By contrast, both WND and PRCP produce cooling trends in the NWPO region. Here, we need to remember that changes of spicing are much weaker than that of heaving in this layer and are subjected to substantial noises from interannual variability (figure 2). Therefore, specific processes through which heat fluxes, winds, and rainfall cause changes in the 23.5–24.5 kg $m^{-3}$ layer is not discussed here.

We then focus on the 26.0–26.7 kg $m^{-3}$ isopycnal layer in which the subsurface cooling occurs. Along-isopycnal cooling trends are all seen in PRCP, WND, and HTFL (figures 7(b)–(f)). A quantitative comparison of these experiments suggests that precipitation change explains 75% of the cooling in the NWPO in CTR. This is in line with existing studies that stressed freshwater fluxes in causing the freshening of the NPIW (Wong *et al* 1999, Durack and Wijffels 2010, Nan *et al* 2015). Increased precipitation first caused a salinity decrease in outcrop zones in the northwestern subpolar Pacific (figures 7(b) and S5, Lu *et al* 2024). Then, these changes spread as density-compensated cooling and freshening signals along the isopycnal surfaces within the North

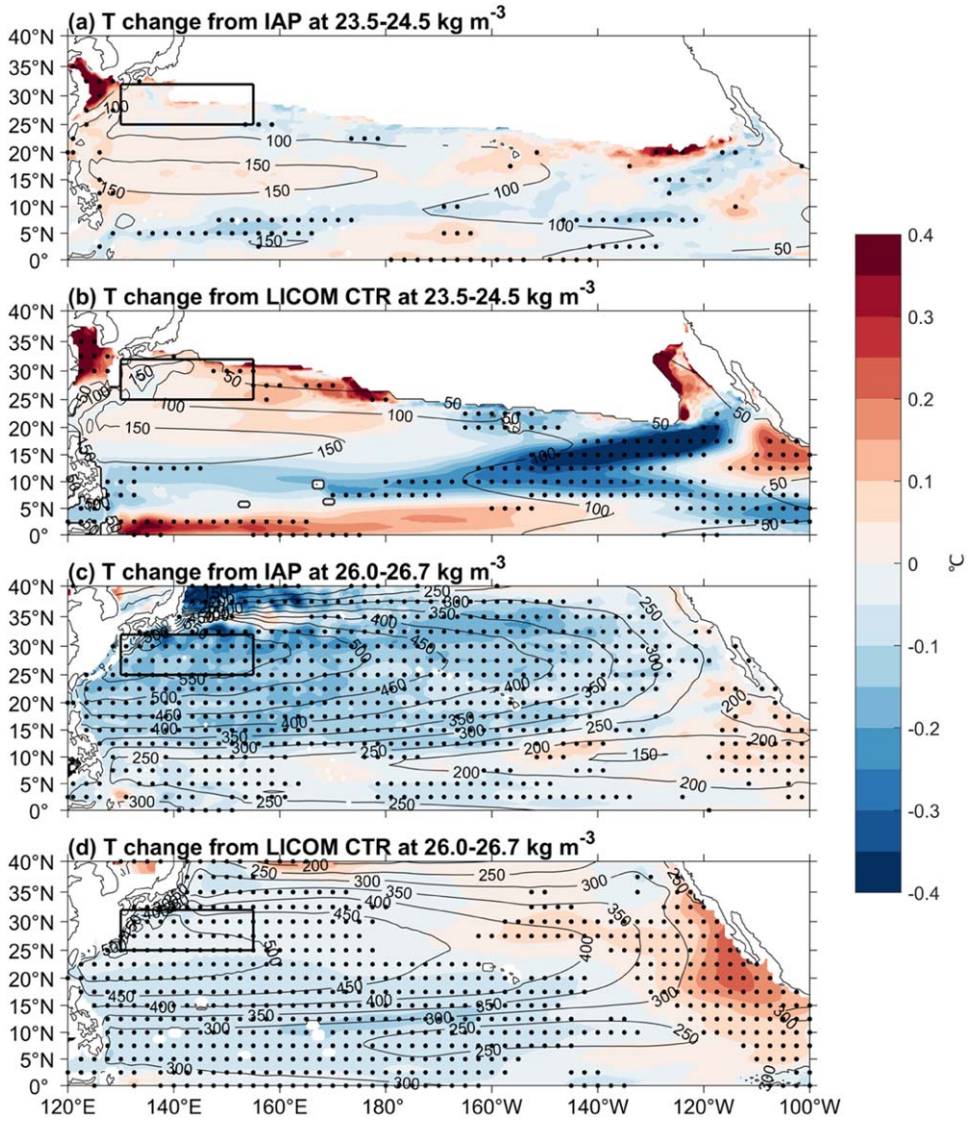


**Figure 6.** Along-isopycnal temperature changes of 1970–2020. Average temperature changes of the 23.5–24.5 kg $m^{-3}$ (a), (b) and 26.0–26.7 kg $m^{-3}$ (c), (d) layers, derived from IAP (a), (c) and LICOM CTR (b), (d). Stippling indicates significant differences at the 90% confidence level. Black contours denote the average depth of the layer in climatology.

Pacific circulation gyres. This process contributes to subsurface cooling in the ECS Kuroshio. Based on various observational data, Nan *et al* (2015) showed that the freshening trend in the NPIW can spread into the Kuroshio through the mean circulation gyre. In comparison with PRCP, the contributions of WND and HTFL are minor. In HTFL, surface heating causes surface warming (figure S5) and density decrease in the North Pacific. This leads to poleward migration of the outcrop zones of NPIW in the subpolar North Pacific, allowing colder and fresher water to subduct into the NPIW (Durack and Wijffels 2010, Lu *et al* 2024).

In summary, the temperature change associated with spicing reflects large-scale property changes of water masses in the North Pacific, driven by buoyancy fluxes in the source regions of these waters and manifesting as density-compensated temperature and salinity changes. The subsurface cooling seen in the ECS Kuroshio mainly arises from the cooling and freshening trends of the NPIW, primarily induced by freshwater uptake and warming-caused migration of its source region under anthropogenic greenhouse warming.

## 4. Remarks

During the past decades, the KC has experienced notable warming trends in its waters. The warming KC brings stress and challenges to ecosystems of the ECS and other surrounding regions. Our study, based on historical hydrographic observation data and ocean model experiments, explores the long-term variation of ECS Kuroshio surface temperature in the ECS from 1970 to 2020, revealing the vertical structure of the ECS Kuroshio and its formation mechanisms. We find that the ECS Kuroshio has significantly warmed in the upper 350 m layer and

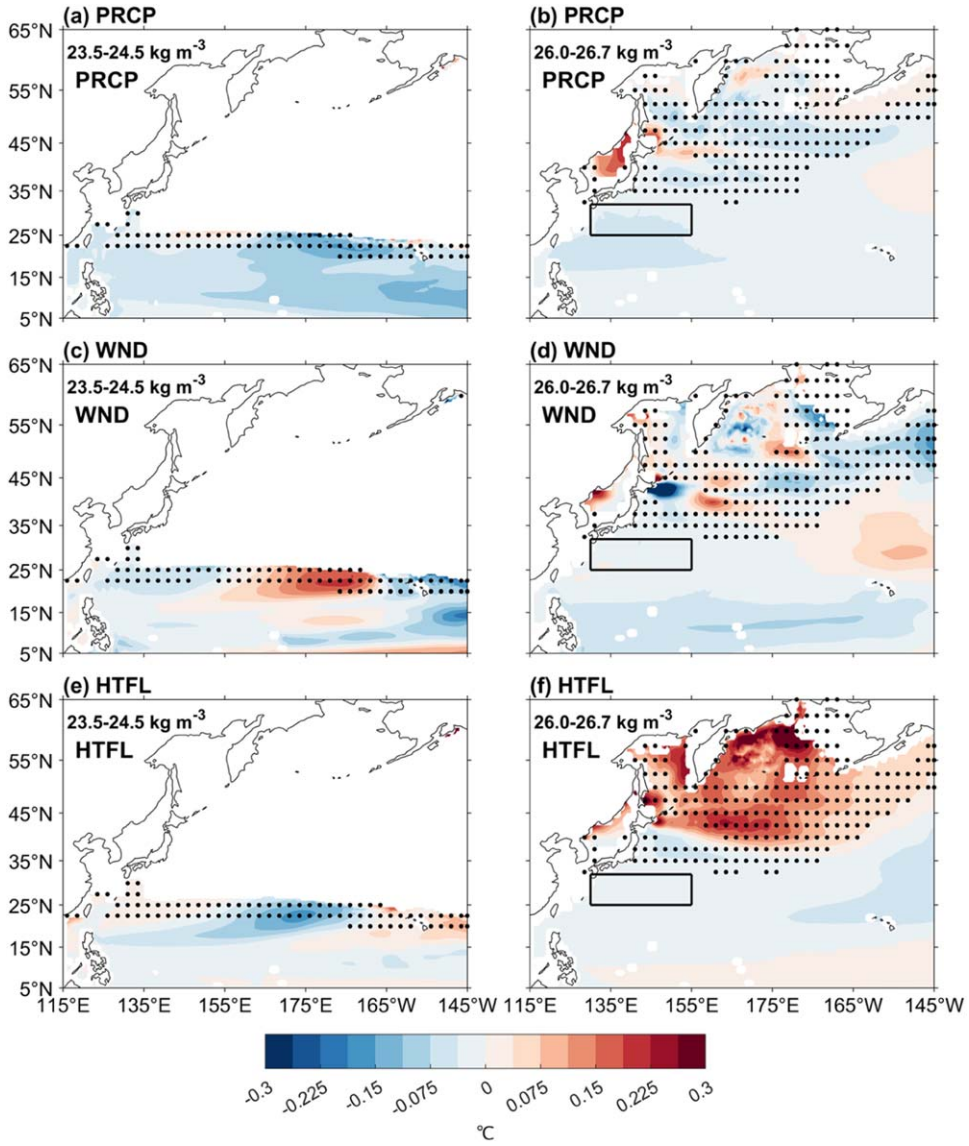


**Figure 7.** Along-isopycnal temperature changes of 1970–2020 in the 23.5–24.5 kg $m^{-3}$ (a), (c,) (e) and 26.0–26.7 kg $m^{-3}$ (b), (d), (f) layers, derived from PRCP (a), (b), WND (c), (d), HTFL (e), (f) simulations of LICOM in spicing. Dots remark the late-winter (March) outcropping regions of the layer.

slightly cooled in the subsurface layer of 350–800 m. Through a diagnosis of heaving and spicing and sensitivity experiments with ocean models, we find different mechanisms governing the upper-layer warming and subsurface cooling. Specifically, the upper-layer warming of the KC is caused by both surface wind changes associated with phase shift of the Pacific Decadal Oscillation (PDO) and surface heating by air-sea heat fluxes. Alternatively, the subsurface cooling, as a manifestation of property changes of the North Pacific Intermediate Water (NPIW), is mainly dictated by buoyancy fluxes in the subpolar northwestern Pacific. This study fills a knowledge gap in understanding the warming structure of the ECS Kuroshio. By linking regional thermal changes in the ECS to large-scale oceanic dynamics and climate changes, these results provide new insights into the response of western boundary currents and continental shelves to anthropogenic climate change.

By revealing the warming structure of the KC and confirming the enhancement of thermal stratification, our work also provides useful implications for understanding biogeochemical and ecosystem changes in the ECS. Studies based on *in situ* observations (Zhang *et al* 2017), numerical models (Zhou *et al* 2015), and biogeochemical tracers (Pei *et al* 2017) suggested that the Kuroshio water invade the ECS shelf across the central ECS continental slope in various years. Changes in thermocline and intermediate waters of the KC may influence the bottom water on the ECS-YS shelf through heat and material exchanges, perturbing the heat budget and biogeochemical cycles of the shelf (Liu et *al* 2021), which is the focus of our on-going research. Also, future effort should be devoted to investigate changes in various water masses of the North Pacific, the drivers, and their environmental impacts on the marginal seas surrounding the KC.

## Acknowledgments

This research is supported by the Laoshan Laboratory (LSKJ202202601), the Strategic Priority Research Program of Chinese Academy of Sciences (XDB40000000), the National Natural Science Foundation of China (Grant 42476025), and the Oceanographic Data Center, Institute of Oceanology, Chinese Academy of Sciences.

## Data availability statement

The data that support the findings of this study are openly available at the following URL/DOI: JMA data: https://www.jodc.go.jp/jodcweb/JDOSS; IAP data: http://www.ocean.iap.ac.cn; CMEMS SSH data: https://data.marine.copernicus.eu/products?facets=mainVariables%7ESea+surface+height; NOAA ETOPO5 data: https://www.ncei.noaa.gov/products/etopo-global-relief-model; PDO Index: https://www.ncei.noaa.gov/access/monitoring/pdo/ and ECMWF ERA5 data: https://cds.climate.copernicus.eu/datasets/reanalysis-era5-single-levels-monthly-means?tab=overview.

## ORCID iDs

Yuanlong Li https://orcid.org/0000-0002-7239-5756
Kai Ge https://orcid.org/0009-0006-9486-6420
Xiaohui Tang https://orcid.org/0000-0002-9809-3561

## References

Andres M, Park J -H, Wimbush M, Zhu X -H, Nakamura H, Kim K and Chang K -I 2009 Manifestation of the Pacific Decadal Oscillation in the Kuroshio *Geophys. Res. Lett.* **36** L16602

Bindoff N L and Mcdougall T J 1994 Diagnosing climate change and ocean ventilation using hydrographic data *J. Phys. Oceanogr.* **24** 1137–52

Bo Q and Lukas R 1996 Seasonal and interannual variability of the North Equatorial Current, the Mindanao Current, and the Kuroshio along the Pacific western boundary *Journal of Geophysical Research: Oceans* **101** 12315–30

Cai R, Tan H and Kontoyiannis H 2017 Robust surface warming in offshore China seas and its relationship to the East Asian monsoon wind field and ocean forcing on interdecadal time scales *J. Clim.* **30** 8987–9005

Cai R, Tan H and Qi Q 2016 Impacts of and adaptation to inter-decadal marine climate change in coastal China seas: impacts of and adaptation to climate change in coastal China seas *Int. J. Climatol.* **36** 3770–80

Chen C-T A, Huang T-H, Wu C-H, Yang H and Guo X 2021 Variability of the nutrient stream near Kuroshio's origin *Sci. Rep.* **11** 5080

Cheng L *et al* 2022 Past and future ocean warming *Nature Reviews Earth & Environment* **3** 776–94

Cheng L *et al* 2024 IAPv4 ocean temperature and ocean heat content gridded dataset *Earth System Science Data* **16** 3517–46

Cheng L, Trenberth K E, Fasullo J, Boyer T, Abraham J and Zhu J 2017 Improved estimates of ocean heat content from 1960 to 2015 *Sci. Adv.* **3** e1601545

Chi L, Song X, Yuan Y, Wang W, Zhou P, Fan X, Cao X and Yu Z 2017 Distribution and key influential factors of dissolved oxygen off the Changjiang River Estuary (CRE) and its adjacent waters in China *Mar. Pollut. Bull.* **125** 440–50

D'Arrigo R, Wilson R, Panagiotopoulos F and Wu B 2005 On the long-term interannual variability of the east Asian winter monsoon *Geophys. Res. Lett.* **32** 2005GL023235

Duan J, Li Y, Cheng L, Lin P and Wang F 2023 Heat storage in the upper indian ocean: the role of wind-driven redistribution *J. Clim.* **36** 2221–42

Durack P J and Wijffels S E 2010 Fifty-year trends in global ocean salinities and their relationship to broad-scale warming *J. Clim.* **23** 4342–62

England M H, McGregor S, Spence P, Meehl G A, Timmermann A, Cai W, Gupta A S, McPhaden M J, Purich A and Santoso A 2014 Recent intensification of wind-driven circulation in the Pacific and the ongoing warming hiatus *Nat. Clim. Change* **4** 222–7

Gao X, Li Y, Lin P, Zhang L, Ren Q, Lu Y and Wang F 2023 Origins of multidecadal SST variations in the southern Atlantic and Indian Oceans since the 1960s *Geophys. Res. Lett.* **50** e2022GL101735

Garuba O A and Klinger B A 2016 Ocean heat uptake and interbasin transport of the passive and redistributive components of surface heating *J. Clim.* **29** 7507–27

Häkkinen S, Rhines P B and Worthen D L 2016 Warming of the global ocean: spatial structure and water-mass trends *J. Clim.* **29** 4949–63

Hersbach H *et al* 2023 ERA5 monthly averaged data on single levels from 1970 to present *Copernicus Climate Change Service (C3S) Climate Data Store (CDS)*

Hsin Y-C, Qiu B, Chiang T-L and Wu. C-R 2013 Seasonal to interannual variations in the intensity and central position of the surface Kuroshio east of Taiwan. *Journal of Geophysical Research: Oceans* **118** 4305–16

Hsueh Y 2000 The Kuroshio in the East China Sea *J. Mar. Syst.* **24** 131–9

Huang B, Thorne P W, Banzon V F, Boyer T, Chepurin G, Lawrimore J H, Menne M J, Smith T M, Vose R S and Zhang H-M 2017 Extended reconstructed sea surface temperature, version 5 (ERSSTv5): upgrades, validations, and intercomparisons *J. Clim.* **30** 8179–205

Huang R X 2020 *Heaving, Stretching and Spicing Modes: Climate Variability in the Ocean* (Springer Singapore) (https://doi.org/10.1007/978-981-15-2941-2)

Kosaka Y and Xie S-P 2013 Recent global-warming hiatus tied to equatorial Pacific surface cooling *Nature* **501** 403–7

Kwon Y-O, Alexander M A, Bond N A, Frankignoul C, Nakamura H, Qiu B and Thompson L A 2010 Role of the Gulf Stream and Kuroshio–Oyashio systems in large-scale atmosphere–ocean interaction: a review *J. Clim.* **23** 3249–81

Li G, Cheng L, Zhu J, Trenberth K E, Mann M E and Abraham J P 2020 Increasing ocean stratification over the past half-century *Nat. Clim. Change* **10** 1116–23

Li X-L, Shi H-M, Xia H-Y, Zhou Y-P and Qiu Y-W 2014 Seasonal hypoxia and its potential forming mechanisms in the Mirs Bay, the northern South China Sea *Cont. Shelf Res.* **80** 1–7
Li Y and Wang F 2012a Spreading and salinity change of North Pacific Tropical Water in the Philippine Sea *J. Oceanogr.* **68** 439–52
Li Y, Wang F and Zhai F 2012b Interannual variations of subsurface spiciness in the Philippine Sea: observations and mechanism *J. Phys. Oceanogr.* **42** 1022–38
Lin P *et al* 2020 LICOM model datasets for the CMIP6 ocean model intercomparison project *Adv. Atmos. Sci.* **37** 239–49
Liu M, Vecchi G, Soden B, Yang W and Zhang B 2021 Enhanced hydrological cycle increases ocean heat uptake and moderates transient climate change *Nat. Clim. Change* **11** 848–53
Liu Z, Gan J, Hu J, Wu H, Cai Z and Deng Y 2021 Progress of studies on circulation dynamics in the East China Sea: the Kuroshio exchanges with the shelf currents *Frontiers in Marine Science* **8** 620910
Lu Y, Li Y, Lin P, Cheng L, Ge K, Liu H, Duan J and Wang F 2024 North Atlantic–Pacific salinity contrast enhanced by wind and ocean warming *Nat. Clim. Change* **14** 723–31
Mantua N J and Hare S R 2002 The Pacific Decadal Oscillation *J. Oceanogr.* **58** 35–44
Miyama T, Nonaka M, Nakamura H and Kuwano-Yoshida A 2012 A striking early-summer event of a convective rainband persistent along the warm Kuroshio in the East China Sea *Tellus A: Dynamic Meteorology and Oceanography* **64** 18962
Nan F, Yu F, Xue H, Wang R and Si G 2015 Ocean salinity changes in the northwest Pacific subtropical gyre: the quasi-decadal oscillation and the freshening trend *Journal of Geophysical Research: Oceans* **120** 2179–92
Nitani H 1972 *Kuroshio: Its Physical Aspects* ed H Stommel and K Yoshida (Univ. Tokyo Press) 129–63
Oey L -Y, Chang M -C, Chang Y -L, Lin Y -C and Xu. F -H 2013 Decadal warming of coastal China Seas and coupling with winter monsoon and currents *Geophys. Res. Lett.* **40** 6288–92
Oka E and Kawabe M 1998 Characteristics of variations of water properties and density structure around the Kuroshio in the East China Sea *J. Oceanogr.* **54** 605–17
Pei Y H, Liu X H and He H L 2017 Interpreting the sea surface temperature warming trend in the Yellow sea and East China Sea *Science China Earth Sciences* **60** 1558–68
Qiao Y-X, Nakamura H, Kako S, Nishina A and Tomita T 2022 Synchronized decadal variabilities in the Kuroshio and Kuroshio Extension system *Prog. Oceanogr.* **204** 102808
Qu T, Kagimoto T and Yamagata T 1997 A subsurface countercurrent along the east coast of Luzon *Deep Sea Res. Part I* **44** 413–23
Ren Q, Kwon Y-O, Yang J, Huang R X, Li Y and Wang F 2024 Substantial warming of the Atlantic Ocean in CMIP6 models *J. Clim.* **37** 3073–3091
Rudnick D, Jan S, Centurioni L, Lee C, Lien R-C, Wang J, Lee D-K, Tseng R-S, Kim Y Y and Chern C-S 2011 Seasonal and mesoscale variability of the Kuroshio near its origin *Oceanography* **24** 52–63
Sasaki Y N and Umeda C 2021 Rapid warming of sea surface temperature along the Kuroshio and the China coast in the East China Sea during the twentieth century *J. Clim.* **34** 4803–4815
Soeyanto E, Guo X, Ono J and Miyazawa Y 2014 Interannual variations of Kuroshio transport in the East China Sea and its relation to the Pacific Decadal Oscillation and mesoscale eddies *Journal of Geophysical Research: Oceans* **119** 3595–616
Tang X, Wang F, Chen Y and Li M 2009 Warming trend in northern East China Sea in recent four decades *Chin. J. Oceanol. Limnol.* **27** 185–91
Trenberth K E, Fasullo J T, Branstator G and Phillips A S 2014 Seasonal aspects of the recent pause in surface warming *Nat. Clim. Change* **4** 911–916
Tsukamoto K 2006 Spawning of eels near a seamount *Nature* **439** 929
Wang F *et al* 2023 The seas around China in a warming climate *Nature Reviews Earth & Environment* **4** 535–51
Wang Y-L, Wu C-R and Chao S-Y 2016 Warming and weakening trends of the Kuroshio during 1993–2013 *Geophysical Research Letters* **43** 9200–7
Wei Y, Huang D and Zhu X-H 2013 Interannual to decadal variability of the Kuroshio Current in the East China Sea from 1955 to 2010 as Indicated by *in-situ* hydrographic data *J. Oceanogr.* **69** 571–89
Wong A P S, Bindoff N L and Church J A 1999 Large-scale freshening of intermediate waters in the Pacific and Indian oceans *Nature* **400** 440–443
Wu C-R 2013 Interannual modulation of the Pacific Decadal Oscillation (PDO) on the low-latitude western North Pacific *Prog. Oceanogr.* **110** 49–58
Wu C-R, Chang Y-L, Oey L-Y, June Chang C-W and Hsin. Y-C 2008 Air-sea interaction between tropical cyclone Nari and Kuroshio *Geophys. Res. Lett.* **35** GL033942 200812
Wu J, Dai M, Xu Y and Zheng J 2019 Plutonium in the western North Pacific: transport along the Kuroshio and implication for the impact of Fukushima Daiichi Nuclear Power Plant accident *Chem. Geol.* **511** 256–64
Wu L *et al* 2012 Enhanced warming over the global subtropical western boundary currents *Nat. Clim. Change* **2** 161–6
Xie S-P, Hafner J, Tanimoto Y, Liu W T, Tokinaga H and Xu H 2002 Bathymetric effect on the winter sea surface temperature and climate of the Yellow and East China Seas *Geophys. Res. Lett.* **29** 81
Xu H, Xu M, Xie S-P and Wang Y 2011 Deep atmospheric response to the spring Kuroshio over the East China Sea *J. Clim.* **24** 4959–72
Xu M, Chang C-P, Fu C, Qi Y, Robock A, Robinson D and Zhang H 2006 Steady decline of east Asian monsoon winds, 1969–2000: Evidence from direct ground measurements of wind speed *Journal of Geophysical Research: Atmospheres* **111** D24111
Yan X, Kang D, Curchitser E N and Pang C 2019 Energetics of Eddy–Mean flow interactions along the western boundary currents in the North Pacific *J. Phys. Oceanogr.* **49** 789–810
Yeh S-W and Kim C-H 2010 Recent warming in the Yellow/East China Sea during winter and the associated atmospheric circulation *Cont. Shelf Res.* **30** 1428–1434
Yu X, Wang F and Tang X 2012 Future projection of East China Sea temperature by dynamic downscaling of the IPCC_AR4 CCSM3 model result *Chinese Journal of Oceanology and Limnology* **30** 826–42
Yuan D, Zhu J, Li C and Hu D 2008 Cross-shelf circulation in the Yellow and East China Seas indicated by MODIS satellite observations *J. Mar. Syst.* **70** 134–49
Zhang J, Guo X, Zhao L, Miyazawa Y and Sun Q 2017 Water exchange across isobaths over the continental shelf of the East China Sea *J. Phys. Oceanogr.* **47** 1043–60
Zhang L, Wu L, Lin X and Wu D 2010 Modes and mechanisms of sea surface temperature low-frequency variations over the coastal China seas *Journal of Geophysical Research: Oceans* **115** 2009JC006025

Zhang Y, John M W and David S B 1997 ENSO-like interdecadal variability: 1900–93 *J. Clim.* **10** 1004–20
Zhang Z-L, Nakamura H and Zhu X-H 2021 Seasonal velocity variations over the entire Kuroshio path part I: data analysis and numerical experiments *J. Oceanogr.* **77** 719–44
Zhou F, Xue H, Huang D, Xuan J, Ni X, Xiu P and Hao Q 2015 Cross-shelf exchange in the shelf of the East China Sea *Journal of Geophysical Research: Oceans* **120** 1545–72
Zhu X, Liu G, Wang J, Wang H, Bao X and Hu W 2015 A numerical study on the relationships of the variations of volume transport around the China seas *J. Mar. Syst.* **145** 15–36